Detection of the Anomalous Velocity with Subpicosecond Time Resolution in Semiconductor Nanostructures

Shekhar Priyadarshi,[*] Klaus Pierz, and Mark Bieler[†]

Physikalisch-Technische Bundesanstalt, 38116 Braunschweig, Germany
(Received 13 July 2015; published 15 December 2015)

We report on the time-resolved detection of the anomalous velocity, constituting charge carriers moving perpendicular to an electric driving field, in undoped GaAs quantum wells. For this we optically excite the quantum wells with circularly polarized femtosecond laser pulses, thereby creating a state which breaks time-inversion symmetry. We then employ a quasi-single-cycle terahertz pulse as an electric driving field to induce the anomalous velocity. The electromagnetic radiation emitted from the anomalous velocity is studied with a subpicosecond time resolution and reveals intriguing results. We are able to distinguish between intrinsic (linked to the Berry curvature) and extrinsic (linked to scattering) contributions to the anomalous velocity both originating from the valence band and observe local energy space dependence of the anomalous velocity. Our results thus constitute a significant step towards noninvasive probing of the anomalous velocity locally in the full energy-momentum space and enable the investigation of many popular physical effects such as the anomalous Hall effect and spin Hall effect on ultrafast time scales.

The movement of charge carriers perpendicular to an electric driving field—even without any magnetic field—constitutes one of the most intriguing properties of carriers in solids. This anomalous movement results in an observable velocity [1] referred to as anomalous velocity $\langle v \rangle_a$ [2–4]. It is at the origin of fascinating physical phenomena [3,5–10], with the spin Hall [5,6] and anomalous Hall [7,9,11] effects being prominent examples, and has direct impact on spintronics [12,13], topological insulators [7,8,14–16], and novel quantum computers [15,17,18]. It is well known that different microscopic effects contribute to $\langle v \rangle_a$ and these are typically divided into intrinsic and extrinsic contributions linked to the Berry curvature ($\boldsymbol{\Omega}$) [2,3,19] and carrier scattering processes [11,20], respectively. However, despite numerous previous studies no straightforward way exists to distinguish between extrinsic and intrinsic contributions [21]. Moreover, being equally important $\langle v \rangle_a$ has not been investigated in the ultrafast regime in which coherence and relaxation processes might have a profound influence on its dynamics.

In this Letter, we report on the detection of $\langle v \rangle_a$ in undoped GaAs quantum wells (QW) with subpicosecond time resolution opening a new area of research for studying the aforementioned physical effects on ultrafast time scales. For this purpose free-space, single-cycle terahertz (THz) pulses are used to accelerate carriers being excited by femtosecond optical pulses in the QWs. This combined optical and THz excitation induces $\langle v \rangle_a$ [3,22–24] on an ultrafast time scale, which, in turn, emits THz radiation into free space. We perform a time-resolved study of this THz emission versus delay between the optical and THz excitation pulses. Our measurements confirm that $\langle v \rangle_a$ results almost entirely from the valence band but also yield two other striking results: (i) The strength of $\langle v \rangle_a$ is significantly influenced by energy relaxation in addition to spin relaxation; (ii) extrinsic effects dominate over intrinsic effects, although we also detect contributions from $\boldsymbol{\Omega}$. This solves an intensively discussed problem on the relative strength of intrinsic and extrinsic effects in GaAs [3,6,25–28].

We first introduce extrinsic and intrinsic contributions to $\langle v \rangle_a$ in more detail. The intrinsic contribution $\langle v \rangle_{a,\mathrm{int}}$ is due to $\boldsymbol{\Omega}$ [29] and has first been theoretically studied in Refs. [1,2,30–32]. The resulting microscopic velocities are proportional to $\mathbf{E} \times \boldsymbol{\Omega}$, with $\mathbf{E}$ being the electric bias field; see Fig. 1(a) [3,19]. The extrinsic contribution $\langle v \rangle_{a,\mathrm{ext}}$ appears due to scattering of carriers with impurities or phonons [11,20,33] and can be divided into three components [33]. The first two components result from coordinate shifts of carriers during scattering events involving symmetric scattering rates. In the first case, such scattering processes induce a microscopic velocity known as side-jump velocity. Upon modification of the momentum-space carrier distribution by the electrical bias the macroscopic side-jump velocity $\langle v \rangle_{a,\mathrm{ext,sj}}$ results; see Fig. 1(b)[11,33]. In the second case carriers lose or gain energy during scattering-induced coordinate shifts along the electrical bias which simultaneously push carriers in momentum space in a direction transverse to the electrical bias. This component is called anomalous carrier distribution and is temporally indistinguishable from $\langle v \rangle_{a,\mathrm{ext,sj}}$. Therefore, in the following discussion we do not distinguish between the anomalous distribution and $\langle v \rangle_{a,\mathrm{ext,sj}}$. The third extrinsic component, referred to as skew scattering $\langle v \rangle_{a,\mathrm{ext,sk}}$, is linked to asymmetric scattering of carriers in momentum space. This effect transfers the electrical-bias-induced asymmetry of the carrier distribution to the direction transverse to the electrical bias; see Fig. 1(c).
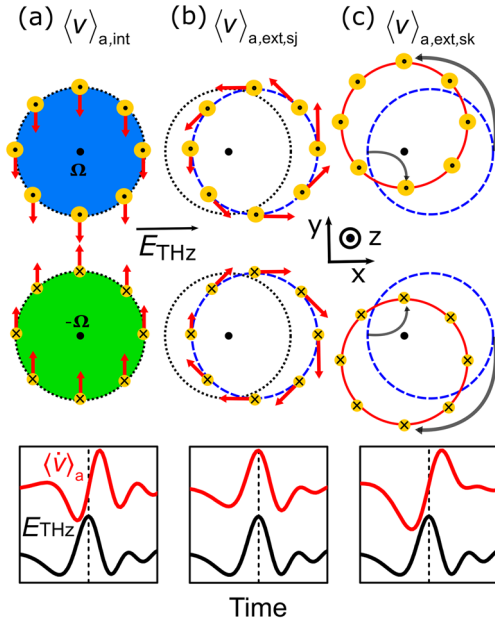
FIG. 1 (color online). Extrinsic and intrinsic contributions. The upper two rows denote two different spin subbands. The third row shows simulated terahertz traces ($\langle \dot{v} \rangle_a$) emitted from the different components of $\langle v \rangle_a$ with respect to the time-dependent electric bias E_{THz}. (a) Intrinsic contribution $\langle v \rangle_{a,int}$ due to the Berry curvature $\boldsymbol{\Omega}$. The blue ($\boldsymbol{\Omega}$) and green ($-\boldsymbol{\Omega}$) colors show Berry curvatures pointing along opposite z directions. The red solid arrows indicate microscopic anomalous velocities (with the arrow length denoting the strength). The black dotted circles represent the energy of carriers being excited with circularly polarized light in one spin subband (without considering spin splitting). The big and small yellow balls indicate large and small density of carriers, respectively. The dots and crosses within the balls indicate spin along $+z$ (spin-up) and $-z$ (spin-down) directions, respectively. (b) Side-jump velocity $\langle v \rangle_{a,ext,sj}$ for the optically excited carrier distribution being displaced by E_{THz}. The blue dashed circles represent the energy of carriers modified by E_{THz}. (c) Skew scattering resulting in $\langle v \rangle_{a,ext,sk}$. The red solid curves represent the energy of carriers modified by scattering processes. The thick (thin) gray arrow denotes the scattering path for carriers from states with large (small) momentum along x to states with large (small) momentum along y. The normal microscopic velocities resulting from the band dispersion are not indicated.

As samples we have chosen (110)- and (001)-oriented, undoped, nominally symmetric GaAs/Al$_{0.3}$Ga$_{0.7}$As QWs, mainly because their band structure and most relevant relaxation times are well known and they are available in a high quality. Moreover, the different orientations exhibit different spin relaxation times which will prove helpful for the data analysis. The (110)-oriented samples have well widths of 8, 15, 18, 24, and 28 nm with the crystallographic directions [001], [1$\bar{1}$0], and [110] taken as the $\hat{x}$, $\hat{y}$, and $\hat{z}$ directions, respectively [34]. The (001)-oriented sample has a well width of 28 nm with the crystallographic directions [1$\bar{1}$0], [110], and [001] taken as the $\hat{x}$, $\hat{y}$, and $\hat{z}$ directions, respectively.

For the generation and detection of $\langle v \rangle_a$ we adopt a recently proposed scheme for probing of $\boldsymbol{\Omega}$ in semiconductor nanostructures [3], but additionally consider extrinsic effects in our data analysis. The output of a femtosecond laser (150 fs long optical pulses whose centre frequency can be tuned between 1.51 and 1.55 eV to excite heavy-hole excitons in our samples) is split into three beams. The first beam (referred to as optical pump beam) with a pulse energy of 2 nJ is circularly polarized and focused to a spot size of $\sim$200 μm exciting a carrier density of $\sim$10^{11} cm^{-2} in the QWs. This excitation creates a state which breaks time-inversion symmetry [3], being a prerequisite for the observation of $\langle v \rangle_a$ in GaAs. The second beam is linearly polarized and used to generate THz pulses E_{THz} via optical rectification in a 2 mm thick (110)-oriented zinc telluride (ZnTe) crystal. These THz pulses act as a time-dependent electric bias. They are focused at normal incidence on the same position of the samples as the optical pump beam yielding a peak electric field inside the sample of $\sim$10 V cm^{-1}. The polarization of E_{THz} is parallel to the $\hat{x}$ axis of the samples as ensured by the orientation of the ZnTe crystal and an additional THz polarizer. The combined optical-THz excitation induces $\langle v \rangle_a$ in the plane of the QWs along the $\hat{y}$ direction. Being induced on an ultrafast time scale, $\langle v \rangle_a$ emits THz radiation, whose electric field is denoted as $\langle \dot{v} \rangle_a$ since it is proportional to the time derivative of $\langle v \rangle_a$ and perpendicularly polarized compared to E_{THz}. The third optical beam, referred to as probe beam, is linearly polarized and used to detect $\langle \dot{v} \rangle_a$ employing electro-optic sampling in a 1 mm thick (110)-oriented ZnTe crystal [35]. In order to suppress E_{THz} and only detect $\langle \dot{v} \rangle_a$ the detection ZnTe crystal is appropriately oriented and two THz polarizers are used. All experiments are performed at 10 K except as explicitly mentioned.

For demonstration of the existence of $\langle v \rangle_a$ we start with experiments on 28 nm (110)-oriented GaAs QWs. In Fig. 2(a) we plot the amplitude of $\langle \dot{v} \rangle_a$ versus delay between the optical and E_{THz} excitation pulses for different helicities of the optical excitation. The helicity of circular polarization of the optical pump determines the spin polarization of carriers [36–38]. Reversing the helicity of the optical pump reverses the spin polarization and, consequently, reverses $\langle v \rangle_a$. Moreover the amplitude of $\langle v \rangle_a$ crucially depends on the delay between the optical and E_{THz} excitation. A slight difference between the two traces shown in Fig. 2(a) appears because of the imperfect suppression of THz signals polarized along the $\hat{x}$ direction [39]. Such signals appear due to THz induced transport of optically excited carriers along the $\hat{x}$ direction being independent of the helicity of the optical pump beam. Therefore, for the remainder of this Letter we always subtract signals resulting from left-handed and right-handed circularly polarized pumps to obtain a background-free signal. The difference between the two curves of Fig. 2(a) is shown in Fig. 2(b). The amplitude of this difference signal is reduced if the polarization of the optical pump beam is changed from circular to elliptical polarization (data not shown), proving that our signal only
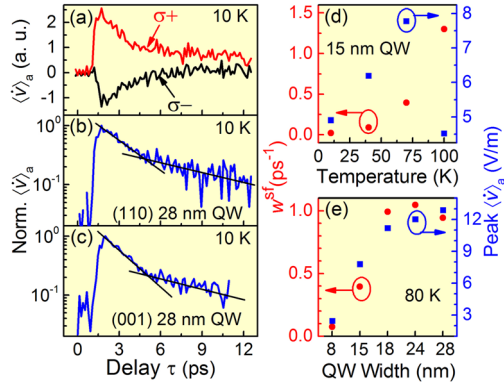
FIG. 2 (color online). (a) Amplitude of the emitted terahertz radiation $\langle v \rangle_a$ from (110)-oriented 28 nm GaAs QWs at 10 K vs delay between optical excitation and E_{THz} for different optical helicities ($\sigma+$ and $\sigma-$). (b) Difference of the delay scans shown in (a), referred to as delay scan, plotted on a logarithmic scale showing a biexponential decay. (c) Delay scan measured in (001)-oriented 28 nm GaAs QWs and plotted on a logarithmic scale showing a biexponential decay. (d) Spin relaxation rates w^{sf} and amplitude of $\langle v \rangle_a$ vs temperature in (110)-oriented 15 nm GaAs QWs. (e) Spin relaxation rates w^{sf} and amplitude of $\langle v \rangle_a$ for different (110)-oriented QWs at 80 K.

appears due to circular polarization of the optical pump beam. Again, in Fig. 2(b) a biexponential decay of the curve is obtained with fast and slow decay rates of $\sim(3 \text{ ps})^{-1}$ and $\sim(10 \text{ ps})^{-1}$, respectively. Repeating the experiments on 15 nm (110)-oriented QWs we obtain decay rates of $\sim(6 \text{ ps})^{-1}$ and $\sim(90 \text{ ps})^{-1}$. We expect that the slow decay rate corresponds to spin relaxation diminishing $\langle v \rangle_a$, since this process destroys spin polarization of carriers and establishes time-inversion symmetry. Therefore, the measured signal has to result from the valence band with previously obtained spin relaxation rates $w^{sf} \approx (50 \text{ ps})^{-1}$ at 4 K [40,41]. We can rule out that $\langle v \rangle_a$ originates from the conduction band, with typical spin relaxation rates of $(300 \text{ ps})^{-1}$ at 10 K [42]. Two other observations confirm this conclusion. First, only a single exponential decay with a rate of $\sim(1 \text{ ps})^{-1}$ is obtained upon increasing the temperature to 100 K; see Fig. 2(d). In contrast, the spin relaxation time in the conduction band of (110)-oriented samples will increase with increasing temperature [42]. Second, the decay rate at 80 K increases with quantum well width; see Fig. 2(e). This can be explained with spin relaxation being enhanced due to band mixing in the valence band which is more pronounced in wider QWs [40].

Having linked the slow decay rate to spin relaxation in the valence band we will now explore the origin of the fast decay rate of the delay scans. In Fig. 2(c) we plot the same delay scan as shown in Fig. 2(b) but measured on (001)-oriented 28 nm GaAs QWs. A very similar dependence with decay rates of $\sim(2 \text{ ps})^{-1}$ and $\sim(9 \text{ ps})^{-1}$ is obtained as compared to the (110) orientation. Therefore, we rule out that momentum relaxation of an optically induced asymmetric hole

distribution, which is present for the (110) orientation but not for the (001) orientation [37,43], is at the main origin of the fast decay rate. Instead we believe that energy relaxation of holes predominantly causes the fast decay, see also the Supplemental Material [44]. This is plausible since $\langle v \rangle_a$ is dependent on carrier energy [3,11,14,54].

So far we have only established the existence of $\langle v \rangle_a$ without being able to distinguish between extrinsic and intrinsic contributions. The existence of $\langle v \rangle_{a,ext}$ is indicated by the dependence of the amplitude of $\langle v \rangle_a$ on temperature [Fig. 2(d)], since $\mathbf{\Omega}$ is not expected to increase with temperature. Yet as shown below a more straightforward way to distinguish between $\langle v \rangle_{a,int}$ and $\langle v \rangle_{a,ext}$ is to analyze the shape of $\langle \dot{v} \rangle_a$. For this purpose we perform delay scans such as the ones plotted in Fig. 2(b) at different temporal instances t of $\langle \dot{v} \rangle_a(t)$. This experiment leads to contour plots for the (001)- and (110)-oriented 28 nm QWs; see Figs. 3(a) and 3(c), respectively. Here, the x and y axes denote the time instance of $\langle \dot{v} \rangle_a$ and the delay between optical and THz excitations, respectively. Comparing the contour plots obtained from the (110)- and (001)-oriented samples with each other, two main features are observed. For the (110) orientation $\langle \dot{v} \rangle_a$ is phase shifted to $E_{THz}(t)$ at early delay times but directly follows $E_{THz}(t)$ at later delay times; see Fig. 3(d). This initial phase shift, which decays with the fast decay rate observed in Fig. 2(b), is considerably reduced in the (001)-oriented GaAs QWs; see Fig. 3(b).

To understand these differences we have to discuss the expected temporal shape of the different intrinsic and extrinsic contributions to $\langle v \rangle_a$. We give a simple intuitive explanation below. A more detailed discussion with the same qualitative results can be found in the Supplemental Material [44]. As introduced earlier $\langle v \rangle_{a,int}$ is proportional to the microscopic velocity given by $\mathbf{E}_{THz} \times \mathbf{\Omega}$, and hence its time dependence can be expressed as $\langle v \rangle_{a,int} \propto E_{THz}(t)$ [3]. Unlike $\langle v \rangle_{a,int}$, which does not require any modification of the carrier distribution by E_{THz}, $\langle v \rangle_{a,ext,sj}$ requires the carrier distribution to be modified by E_{THz}, see Fig. 1(b). This modified carrier distribution ρ relaxes to equilibrium due to scattering with impurities or phonons. The corresponding dynamic equation is given by $\dot{\rho} + w_{\mathbf{k}}^s \rho \propto E_{THz}$, with $w_{\mathbf{k}}^s$ being the symmetric scattering rate and ignoring the much smaller asymmetric scattering rate $w_{\mathbf{k}}^a$ [20]. This yields $\langle v \rangle_{a,ext,sj} \propto \rho \propto \{E_{THz} * [u(t) \exp(-w_{\mathbf{k}}^s t)]\}$, with $u(t)$ being the step function and $*$ denoting convolution. Skew scattering is linked to asymmetric scattering for which the carriers are scattered preferably in a certain direction. Consequently, the whole distribution will be shifted along this direction. However, the equilibrium distribution does not contribute to $\langle v \rangle_{a,ext,sk}$, only the nonequilibrium carrier distribution ρ which is already modified by E_{THz} will be rotated at right angles due to skew scattering; see Fig. 1(c). The dynamics of the skew-scattered carrier distribution ρ_{sk} is given by the equation $\dot{\rho}_{sk} + w_{\mathbf{k}}^s \rho_{sk} = w_{\mathbf{k}}^a \rho$. This yields $\langle v \rangle_{a,ext,sk} \propto \rho_{sk} \propto w_{\mathbf{k}}^a \{E_{THz} * [u(t) t \exp(-w_{\mathbf{k}}^s t)]\}$. In
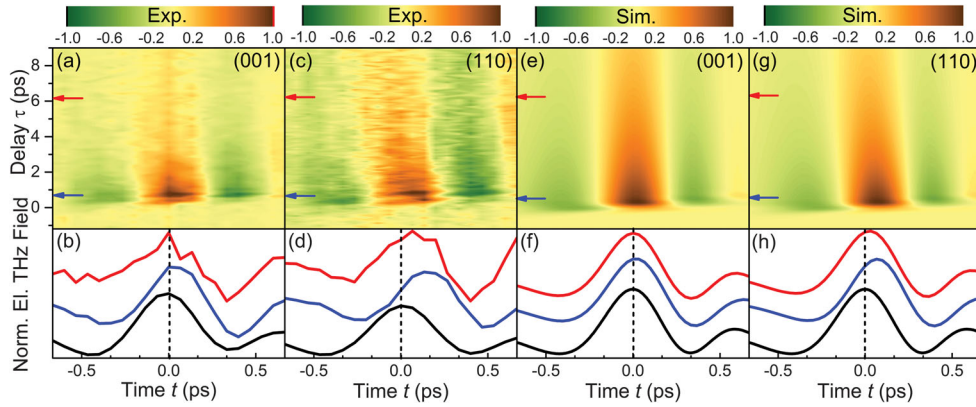
FIG. 3 (color). Upper row: Shown are contour plots in which $\langle v \rangle_a$ is plotted vs time (x axis) and delay between the optical and E_{THz} excitation pulses (y axis) in (001)-oriented 28 nm GaAs QWs (a) and (110)-oriented 28 nm GaAs QWs (c). Lower row: The black curves indicate the shape of E_{THz} after electro-optic detection, while the blue and red curves denote $\langle v \rangle_a$ at early and late delay of the corresponding contour plots, respectively. The corresponding delay times are indicated in the contour plots with horizontal arrows. (e)–(h) show simulations of the experimental results plotted in (a)–(d), respectively.

our simple model given here and in Ref. [44], we ignore Coulomb interaction. Coulomb interaction between electrons (or holes) with opposite spins is responsible for the Coulomb drag effect [20]. However, this effect is not important in our case since we excite spin-polarized carriers.

Our simple analysis clearly shows that the shape of $\langle v \rangle_a$ and, therefore, also of $\langle \dot{v} \rangle_a$, will differ significantly for their various components. For symmetric scattering rates lying in the picosecond range, $\langle \dot{v} \rangle_{a,int}$ and $\langle \dot{v} \rangle_{a,ext,sk}$ peak at times where $E_{THz}(t)$ is zero, while $\langle v \rangle_{a,ext,sj}$ almost directly follows E_{THz}; see last row of Fig. 1. Comparing these expected temporal shapes of $\langle \dot{v} \rangle_a$ with the measured shapes of Figs. 3(b) and 3(d), a striking conclusion can be made. In (001)-oriented samples the main contribution to $\langle v \rangle_a$ arises from $\langle v \rangle_{a,ext,sj}$ and not from $\langle v \rangle_{a,int}$ as previously assumed in Refs. [3,25–28,55]. Only in (110)-oriented samples $\langle v \rangle_{a,int}$ and/or $\langle v \rangle_{a,ext,sk}$ seem to significantly contribute to $\langle v \rangle_a$, especially at early time delays. Before discussing these contributions we like to point out the influence of energy relaxation on $\langle v \rangle_{a,ext,sj}$. In the (001)-oriented sample where the phase shift of $\langle \dot{v} \rangle_a$ as compared to E_{THz} is small the biexponential decay of the delay scan [Fig. 2(c)] has to be caused by $\langle v \rangle_{a,ext,sj}$. Thus, $\langle v \rangle_{a,ext,sj}$ not only depends on spin polarization but also on energy and momentum [11]. The fact that this dependence becomes clearly visible in our results confirms the strength of our experimental technique and paves the way for local (energy space) probing of $\langle v \rangle_a$.

We will now argue that the initial phase shift of $\langle \dot{v} \rangle_a$ in the (110)-oriented samples results from $\langle v \rangle_{a,int}$. In principle, both $\langle v \rangle_{a,int}$ and $\langle v \rangle_{a,ext,sk}$ will lead to a phase shift of $\langle \dot{v} \rangle_a$ as compared to E_{THz}. However, the contribution from $\langle v \rangle_{a,ext,sk}$ will be considerably slower than the contribution from $\langle v \rangle_{a,int}$, see Fig. 1, and, thus, lead to stretched THz traces. We do not observe THz traces which are stretched as compared to E_{THz}, but rather compressed in time, see Fig. 3(d). This observations can only be explained by

considering $\langle v \rangle_{a,int}$, proving the existence of this component. Since $\mathbf{\Omega}$ of the first heavy-hole state is zero at $\mathbf{k} = 0$ [3,54], $\langle v \rangle_{a,int}$ will predominantly vanish with energy relaxation and not with spin relaxation as $\langle v \rangle_{a,ext,sj}$. We believe that this is the reason why the phase shift of $\langle \dot{v} \rangle_a$ decreases with increasing delay. We can rule out that the biexponential decay of the delay scans is predominantly caused by biexponential energy relaxation [56]. In such a case the contour plot and individual THz traces shown in Figs. 3(c) and 3(d) will not show any delay-dependent phase shift.

Simulations based on above arguments considering $\langle v \rangle_{a,int}$ and $\langle v \rangle_{a,ext,sj}$ are plotted in Figs. 3(e)–3(h); see Ref. [44]. The simulations show very good resemblance with the experiments and provide ratios $(\langle v \rangle_{a,int}/\langle v \rangle_{a,ext,sj}) \sim$ 0.04 and $(\langle v \rangle_{a,int}/\langle v \rangle_{a,ext,sj}) \sim 0.6$ for (001)-oriented and (110)-oriented GaAs QWs, respectively. Although we cannot fully rule out that also $\langle v \rangle_{a,ext,sk}$ contributes to $\langle v \rangle_a$, all features of the experimental results can be explained without considering $\langle v \rangle_{a,ext,sk}$. The stronger intrinsic contribution to $\langle v \rangle_a$ in the (110)-oriented samples compared to (001)-oriented samples can be attributed to band mixing in the valence band [3,54]. Band mixing is known to enhance $\mathbf{\Omega}$ and it is stronger in (110)-oriented than in (001)-oriented GaAs QWs [43]. Band mixing also enhances the overall anomalous velocity response which is apparent from the increasing amplitude of $\langle \dot{v} \rangle_a$ with increasing quantum well width of the (110)-oriented samples; see Fig. 2(e) [3,54]. We have also measured similar behavior in (001)-oriented GaAs QWs.

Finally, we comment on small oscillations, which are superimposed on the delay scans at very early time delays, see Figs. 3(a) and 3(c). We believe that the oscillations with a frequency of ∼3 THz appear because of the presence of a shift current component [4] being 2nd order in the optical field and first order in THz field. We have ruled out that

the oscillations are due to plasma, Rabi, or Zitterbewegung effects. In any case it should be emphasized that the oscillations vanish within ∼0.6 ps while the phase shift of $\langle v \rangle_a$ persists for several picoseconds. In fact, in (110)-oriented QWs we even observe a phase shift after 6 ps time delay; see Fig. 3(d) confirming that the observed phase shift is not an artifact appearing due to the aforementioned oscillations.

In conclusion, we have detected $\langle v \rangle_a$ showing a subpicosecond time response in GaAs QWs. We not only identified $\langle v \rangle_{a,\text{int}}$ and $\langle v \rangle_{a,\text{ext,sj}}$ contributions but could also estimate their relative strengths. This study shows that even in a clean and cold semiconductor extrinsic effects may not be ignored and may even constitute the major contribution to $\langle v \rangle_a$. Our observations will have important implications on work regarding Berry curvature and spin transports in semiconductors and might find applications in future ultrafast spintronic devices. Finally, we note that the time-resolved detection of $\langle v \rangle_a$ as advocated in this work can be applied to a wide range of materials enabling direct probing of topological properties.

---

[*]shekhar.priyadarshi@chemie.uni-hamburg.de
Present address: Institute of Physical Chemistry, University of Hamburg, 20146 Hamburg, Germany.
[†]mark.bieler@ptb.de

[1] R. Karplus and J. M. Luttinger, Hall effect in ferromagnetics, Phys. Rev. **95**, 1154 (1954).

[2] E. N. Adams and E. I. Blount, Energy bands in the presence of an external force field-II. Anomalous velocities, J. Phys. Chem. Solids **10**, 286 (1959).

[3] K. S. Virk and J. E. Sipe, Optical Injection and Terahertz Detection of the Macroscopic Berry Curvature, Phys. Rev. Lett. **107**, 120403 (2011).

[4] C. Aversa and J. E. Sipe, Nonlinear optical susceptibilities of semiconductors: Results with a length-gauge analysis, Phys. Rev. B **52**, 14636 (1995).

[5] S. Murakami, N. Nagaosa, and S. Zhang, Dissipationless quantum spin current at room temperature, Science **301**, 1348 (2003).

[6] Y. K. Kato, R. C. Myers, A. C. Gossard, and D. D. Awschalom, Observation of the spin hall effect in semiconductors, Science **306**, 1910 (2004).

[7] R. Yu, W. Zhang, H.-J. Zhang, S.-C. Zhang, X. Dai, and Z. Fang, Quantized anomalous hall effect in magnetic topological insulators, Science **329**, 61 (2010).

[8] Y. Zhang, Y.-W. Tan, H. L. Stormer, and P. Kim, Experimental observation of the quantum Hall effect and Berry's phase in graphene, Nature (London) **438**, 201 (2005).

[9] W.-L. Lee, S. Watauchi, V. L. Miller, R. J. Cava, and N. P. Ong, Dissipationless anomalous hall current in the ferromagnetic spinel $CuCr_2Se_{4-x}Br_x$, Science **303**, 1647 (2004).

[10] H. Kurebayashi, J. Sinova, D. Fang, A. C. Irvine, T. D. Skinner, J. Wunderlich, V. Nova'k, R. P. Campion, B. L. Gallagher, E. K. Vehstedt, L. P. Zarbo, K. Vyborny, A. J. Ferguson, and T. Jungwirth, An antidamping spin—orbit torque originating from the Berry curvature, Nat. Nanotechnol. **9**, 211 (2014).

[11] N. A. Sinitsyn, Semiclassical theories of the anomalous Hall effect, J. Phys. Condens. Matter **20**, 023201 (2008).

[12] J. Wunderlich, a. C. Irvine, J. Sinova, B. G. Park, L. P. Zârbo, X. L. Xu, B. Kaestner, V. Novák, and T. Jungwirth, spin-injection hall effect in a planar photovoltaic cell, Nat. Phys. **5**, 675 (2009).

[13] T. Kampfrath, M. Battiato, P. Maldonado, G. Eilers, J. Nötzold, S. Mährlein, V. Zbarsky, F. Freimuth, Y. Mokrousov, S. Blügel, M. Wolf, I. Radu, P. M. Oppeneer, and M. Münzenberg, Terahertz spin current pulses controlled by magnetic heterostructures, Nat. Nanotechnol. **8**, 256 (2013).

[14] W. Yao, A. H. MacDonald, and Q. Niu, Optical Control of Topological Quantum Transport in Semiconductors, Phys. Rev. Lett. **99**, 047401 (2007).

[15] D. Hsieh, Y. Xia, L. Wray, D. Qian, a. Pal, J. H. Dil, J. Osterwalder, F. Meier, G. Bihlmayer, C. L. Kane, Y. S. Hor, R. J. Cava, and M. Z. Hasan, Observation of unconventional quantum spin textures in topological insulators, Science **323**, 919 (2009).

[16] P. Hosur, Circular photogalvanic effect on topological insulator surfaces: Berry-curvature-dependent response, Phys. Rev. B **83**, 035309 (2011).

[17] P. J. Leek, J. M. Fink, A. Blais, R. Bianchetti, M. Göppl, J. M. Gambetta, D. I. Schuster, L. Frunzio, R. J. Schoelkopf, and A. Wallraff, Observation of Berry's phase in a solid-state qubit, Science **318**, 1889 (2007).

[18] D. D. Awschalom, D. Loss, and N. Samarth, *Semiconductor Spintronics and Quantum Computation* (Springer, Berlin, 2002).

[19] M. Gradhand, D. V Fedorov, F. Pientka, P. Zahn, I. Mertig, and B. L. Györffy, First-Principle calculations of the Berry curvature of Bloch states for charge and spin transport of electrons, J. Phys. Condens. Matter **24**, 213202 (2012).

[20] E. M. Hankiewicz and G. Vignale, Spin-Hall effect and spin-coulomb drag in doped semiconductors, J. Phys. Condens. Matter **21**, 253202 (2009).

[21] C. Zeng, Y. Yao, Q. Niu, and H. H. Weitering, Linear Magnetization Dependence of the Intrinsic Anomalous Hall Effect, Phys. Rev. Lett. **96**, 037204 (2006).

[22] F. Yang, X. Xu, and R.-B. Liu, Giant Faraday rotation induced by the Berry phase in bilayer graphene under strong terahertz fields, New J. Phys. **16**, 043014 (2014).

[23] F. Yang and R.-B. Liu, Berry phases of quantum trajectories of optically excited electron–hole pairs in semiconductors under strong terahertz fields, New J. Phys. **15**, 115005 (2013).

[24] F. Yang and R.-B. Liu, Nonlinear optical response induced by non-Abelian Berry curvature in time-reversal-invariant insulators, Phys. Rev. B **90**, 245205 (2014).

[25] J. Wunderlich, B. Kaestner, J. Sinova, and T. Jungwirth, Experimental Observation of the Spin-Hall Effect in a Two-Dimensional Spin-Orbit Coupled Semiconductor System, Phys. Rev. Lett. **94**, 047204 (2005).

[26] L. K. Werake, B. A. Ruzicka, and H. Zhao, Observation of Intrinsic Inverse Spin Hall Effect, Phys. Rev. Lett. **106,** 107205 (2011).

[27] S. Murakami, Absence of vertex correction for the spin Hall effect in p-type semiconductors, Phys. Rev. B **69,** 241202 (2004).

[28] B. A. Bernevig and S.-C. Zhang, Intrinsic Spin Hall Effect in the Two-Dimensional Hole Gas, Phys. Rev. Lett. **95,** 016801 (2005).

[29] M. V. Berry, Quantal phase factors accompanying adiabatic changes, Proc. R. Soc. A **392,** 45 (1984).

[30] J. M. Luttinger and W. Kohn, Motion of electrons and holes in perturbed periodic fields, Phys. Rev. **97,** 869 (1955).

[31] J. M. Luttinger, Theory of the Hall Effect in ferromagnetic substances, Phys. Rev. **112,** 739 (1958).

[32] E. I. Blount, *Formalisms of Band Theory*, (Academic Press, New York and London, 1962).

[33] V. I. Belinicher, E. L. Ivchenko, and B. I. Sturman, Kinetic theory of the displacement photovoltaic effect in piezo-electrics, Sov. Phys. JETP **56,** 359 (1982).

[34] S. Priyadarshi, M. Leidinger, K. Pierz, A. M. Racu, U. Siegner, M. Bieler, and P. Dawson, Terahertz spectroscopy of shift currents resulting from asymmetric (110)-oriented GaAs/AlGaAs quantum wells, Appl. Phys. Lett. **95,** 151110 (2009).

[35] X. C. Zhang, Y. Jin, and X. F. Ma, Coherent measurement of THz optical rectification from electro-optic crystals, Appl. Phys. Lett. **61,** 2764 (1992).

[36] S. Priyadarshi, K. Pierz, and M. Bieler, All-Optically Induced Ultrafast Photocurrents: Beyond the Instantaneous Coherent Response, Phys. Rev. Lett. **109,** 216601 (2012).

[37] E. L. Ivchenko and S. A. Tarasenko, Pure spin photocurrents, Semicond. Sci. Technol. **23,** 114007 (2008).

[38] S. D. Ganichev and W. Prettl, Spin photocurrents in quantum wells, J. Phys. Condens. Matter **15,** R935 (2003).

[39] C. B. Schmidt, S. Priyadarshi, S. A. Tarasenko, and M. Bieler, Ultrafast magneto-photocurrents in GaAs: Separation of surface and bulk contributions, Appl. Phys. Lett. **106,** 142108 (2015).

[40] T. Ostatnický, O. Crégut, M. Gallart, P. Gilliot, B. Hönerlage, and J.-P. Likforman, Electron- and hole-spin relaxation within excitons in GaAs quantum wells by nondegenerate pump-and-probe measurements, Phys. Rev. B **75,** 165311 (2007).

[41] S. D. Ganichev, S. N. Danilov, V. V. Bel'kov, E. L. Ivchenko, M. Bichler, W. Wegscheider, D. Weiss, and W. Prettl, Spin-Sensitive Bleaching and Monopolar Spin Orientation in Quantum Wells, Phys. Rev. Lett. **88,** 057401 (2002).

[42] Y. Ohno, R. Terauchi, T. Adachi, F. Matsukura, and H. Ohno, Spin Relaxation in GaAs (110) Quantum Wells, Phys. Rev. Lett. **83,** 4196 (1999).

[43] H. T. Duc, J. Förstner, and T. Meier, Microscopic analysis of charge and spin photocurrents injected by circularly polarized one-color laser pulses in GaAs quantum wells, Phys. Rev. B **82,** 115316 (2010).

[44] See Supplemental Material at http://link.aps.org/supplemental/10.1103/PhysRevLett.115.257401 for the microscopic model of the anomalous velocity, which includes Refs. [45–53].

[45] J. E. Sipe and A. I. Shkrebtii, Second-order optical response in semiconductors, Phys. Rev. B **61,** 5337 (2000).

[46] S. Priyadarshi, K. Pierz, and M. Bieler, Accessing new types of photocurrents using polarization-shaped excitation pulses, Proc. SPIE Int. Soc. Opt. Eng. **8623,** 86231B (2013).

[47] S. Priyadarshi, K. Pierz, and M. Bieler, All-optically induced currents resulting from frequency-modulated coherent polarization, Appl. Phys. Lett. **102,** 112102 (2013).

[48] R. D. R. Bhat and J. E. Sipe, Optically Injected Spin Currents in Semiconductors, Phys. Rev. Lett. **85,** 5432 (2000).

[49] M. I. Bakunov, S. B. Bodrov, A. V. Maslov, and M. Hangyo, Theory of terahertz generation in a slab of electro-optic material using an ultrashort laser pulse focused to a line, Phys. Rev. B **76,** 085346 (2007).

[50] A. Tomasino, A. Parisi, S. Stivala, P. Livreri, A. C. Cino, A. C. Busacca, M. Peccianti, and R. Morandotti, Wideband THz time domain spectroscopy based on optical rectification and electro-optic sampling, Sci. Rep. **3,** 3116 (2013).

[51] A. Nahata, A. S. Weling, and T. F. Heinz, A wideband coherent terahertz spectroscopy system using optical rectification and electro-optic sampling, Appl. Phys. Lett. **69,** 2321 (1996).

[52] G. Gallot, J. Zhang, R. W. McGowan, T.-I. Jeon, and D. Grischkowsky, Measurements of the THz absorption and dispersion of znte and their relevance to the electro-optic detection of thz radiation, Appl. Phys. Lett. **74,** 3450 (1999).

[53] G. Gallot and D. Grischkowsky, Electro-optic detection of terahertz radiation, J. Opt. Soc. Am. B **16,** 1204 (1999).

[54] W. Yao and Q. Niu, Berry Phase Effect on the Exciton Transport and on the Exciton Bose-Einstein Condensate, Phys. Rev. Lett. **101,** 106401 (2008).

[55] J. L. Yu, Y. H. Chen, Y. Liu, C. Y. Jiang, H. Ma, L. P. Zhu, and X. D. Qin, Intrinsic photoinduced Anomalous Hall effect in insulating GaAs/AlGaAs quantum wells at room temperature, Appl. Phys. Lett. **102,** 202408 (2013).

[56] H. F. Tiedje, H. K. Haugen, and J. S. Preston, Measurement of nonlinear absorption coefficients in GaAs, InP and Si by an optical pump THz probe technique, Opt. Commun. **274,** 187 (2007).